14

Application of piezoelectric ceramics in pulsed power technology and engineering

Sergey I. Shkuratov[1], Evgueni F. Talantsev[2] and Jason Baird[1,3]
[1]*Loki Incorporated, Rolla, MO 65409,*
[2]*Pulsed Power LLC, Lubbock, TX 79416,*
[3]*Department of Mining and Nuclear Engineering, Missouri University of Science and Technology, Rolla, MO 65409-0450,*
U.S.A.

1. Introduction

Poled ferroelectrics are capable of storing electromagnetic energy in a form of bonded electric charge. The electric charge density of poled lead zirconate titanate (PZT) ceramic samples can exceed 30 μC/cm^2 and the electromagnetic energy density stored in the samples can reach 4 J/cm^3. Releasing the electric charge stored in ferroelectrics during a microsecond time interval can generate pulses of high voltage, high current and high power. The generation of pulsed voltage and pulsed currents by shock-compressed lead zirconate titanate and barium titanate ferroelectric ceramics was reported for the first time at the end of the 1950s (Neilson, 1957). Studies of the physical and electrical properties of shock-compressed ferroelectric and piezoelectric materials with light gas guns and explosively accelerated pellets, which initiated planar shock waves in the investigated samples have been performed since the 1960s and continue until present time (Reynolds & Seay, 1961; Reynolds & Seay, 1962; Halpin, 1966; Cutchen, 1966; Halpin, 1968; Lysne, 1973; Lysne & Percival, 1975; Lysne, 1975; Lysne & Percival, 1976; Bauer & Vollrath, 1976a; Bauer & Vollrath, 1976b; Mineev & Ivanov, 1976; Duvall & Graham, 1977; Lysne, 1977; Novitskii, et al., 1978; Dick & Vorthman, 1978; Dungan & Storz, 1985; Novitskii & Sadunov, 1985; Setchell, 2003; Setchell, 2005; Setchell et al., 2006; Setchell, 2007).
Since 1990s we have been performing design work, experimental studies (Shkuratov et al., 2004; Shkuratov et al., 2006a; Shkuratov et al., 2006c; Shkuratov et al., 2007a; Shkuratov et al., 2007b; Shkuratov et al., 2007c; Shkuratov et al., 2007d; Shkuratov et al., 2008a; Shkuratov et al., 2008b; Shkuratov et al., 2010) and theoretical investigations (Tkach et al., 2002, Shkuratov et al., 2007d; Shkuratov et al., 2008a) of miniature pulsed power generators based on shock depolarization of ferroelectric materials. Development of these autonomous prime power sources is important for the success of modern research and development projects (Altgilbers et al., 2009; Altgilbers et al., 2010).
Results of systematic studies of miniature ferroelectric generators (FEGs) are presented in this chapter. We describe the design of a miniature FEG, consider principles of its operation,

give examples of performance of the generators in the high resistance and charging modes, and operation of the FEG equipped with a power conditioning stage.

2. Explosively Driven Ferroelectric Generator Design

A schematic diagram of our miniature shock wave FEGs that was used in experimental studies described in this chapter (Shkuratov et al., 2004; Shkuratov et al., 2006a; Shkuratov et al., 2006c; Shkuratov et al., 2008a) is shown in Fig. 1. It contained a ferroelectric element, an explosive chamber, a metallic impactor (flyer plate) and output terminals. The explosive part of the FEG contained a plastic cylindrical detonator support that holds an RP-501 detonator (supplied by RISI (Online A)) and a high explosive charge. The air gap between the flyer plate and the ferroelectric element front contact plate (the acceleration path) was 5 mm.

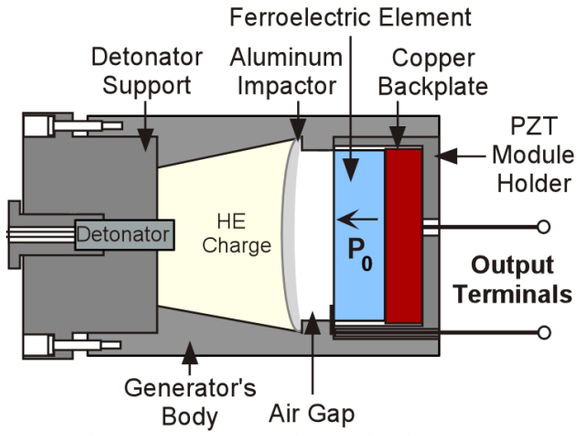

Fig. 1. A schematic diagram of a miniature explosively driven shock wave ferroelectric generator (FEG).

The metallic impactor was responsible for initiation of a shock wave in the ferroelectric element. A flyer plate accelerated to high velocity by the detonation of a high explosive charge impacted the face plate of the ferroelectric element and initiated a shock wave in the body of the ferroelectrics. The direction of propagation of shock wave in the ferroelectric element was parallel to the polarization vector $\boldsymbol{P_0}$ (Fig. 1). This type of generator is referred to as a longitudinal FEG. The overall dimensions of the FEGs did not exceed 50 mm.
Desensitized RDX (essentially the same as Composition 4, or C-4) high explosives were used in all FEGs described in this chapter. The detonation velocity of desensitized RDX is 8.04 km/s and the dynamic pressure at the shock front reaches 36.7 GPa. The mass of the C-4 charge was varied from 12 to 17 g, depending on the charge holder configurations.
To provide a planar impact in the ferroelectric element, we designed the impactor (Fig. 1) as a curved plate that deformed into a quasi-flat structure under blast loads. To derive the correct curvature and thickness of the flyer plate material, the arrival times and locations of the explosive shock was calculated based on the principles of geometric optics and impedance mismatch as applied to detonation waves. Then, the shock transit time through the flyer plate material was calculated in order to calculate shock time of arrival along concentric circular loci on the target side of the flyer plate. The combination of shock arrival

times and locations on the plate surface allowed for calculation of the plate curvature needed to produce an essentially flat flyer plate upon impact with the PZT target.
The cylindrical body of the FEG was made of material with good electrical insulating characteristics to avoid electric breakdown during the operation of the generator. We performed a series of experimental studies to determine the effects of generator body material on the explosive and electrical operation of the FEG (Shkuratov et al., 2004; Shkuratov et al., 2006c). Three types of plastics were used for the generator bodies: polyethylene, polyvinylchloride (PVC) and polycarbonate. The experimental results showed that each of these materials worked well.
In addition, we performed a series of experimental investigations to determine the effect of generator body wall thickness on the electrical operation of the FEG (Shkuratov et al., 2004; Shkuratov et al., 2006c). As a result of these studies it was found, that there is no significant difference in the generation of high-voltage pulses by FEGs having body wall thicknesses in the range from 1 mm to 30 mm. Based on this result, we reduced the total volume of the FEGs for four times. Physics behind this result is related to the fact that the generator's body does not effect on the explosive and electrical operation of the FEG, it only holds the ferroelectric element and explosive part together until detonation of the high explosives. The generator's body can be a lightweight and thin plastic shell (less than a millimeter larger than the diameter of the ferroelectric element).

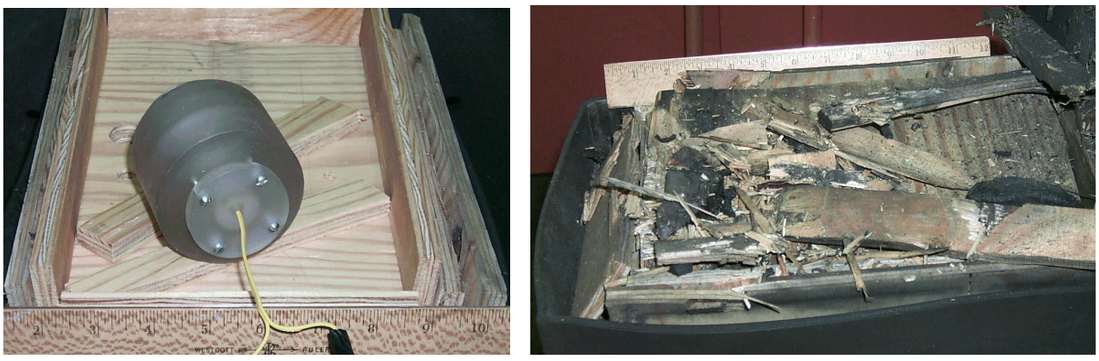

A B

Fig. 2. Shock wave ferroelectric generator before (A) and after (B) explosive and electrical operation.

The ferroelectric element (Fig. 1) was bonded to a copper back-plate that was 1 mm larger in diameter than the ferroelectric element. The back-plate thickness was 5 mm. A silver-loaded epoxy was used to bond the ferroelectric disk to the back-plate. The copper back-plate provided mechanical impedance matching for minimizing reflection of the stress wave when it reached the back face of the ferroelectric energy-carrying element. The silver-loaded epoxy provided an electrical contact and reduced the capacitive reactance of the bond to a negligible value. The ferroelectric element, along with the copper back-plate, was centered in a cylindrical plastic holder (Fig. 1).
Two output electric terminals of the FEG were connected to two contact leads that were connected to the metallic contact plates deposited on the surface of the ferroelectric disk. One contact lead was bonded to the front plate of the ferroelectric disk (which was subjected to flyer plate impact) with silver-loaded epoxy. Another lead was bonded in the same

manner to the copper back-plate. Figure 2 shows an FEG before and after explosive detonation and electrical operation.

3. Generation of Pulsed High Voltage by Longitudinally-Shock-Compressed PZT 52/48 Ferroelectrics

There are well known difficulties in the generation of pulsed power in a high resistance load with explosively driven electrical generators (including all types of magnetic flux compression generators, magneto-hydrodynamic generators, etc.) (Altgilbers et al., 2010). We demonstrated in a series of systematic experimental studies that explosively driven longitudinal FEGs are an exception to this list (Shkuratov et al., 2004; Shkuratov et al., 2006a; Shkuratov et al., 2006c; Shkuratov et al., 2008a; Shkuratov et al., 2008b). FEGs are explosively driven pulsed power sources that effectively generate high voltage across high-resistance loads.

In these studies we used lead zirconate titanate $Pb(Zr_{0.52}Ti_{0.48})O_3$ (PZT 52/48) poled piezoelectric ceramics (trade mark EC-64, supplied by ITT Corp. (Online B)). PZT 52/48 is a ferroelectric material widely used in modern mechanical and electrical systems due to its excellent piezoelectric properties. This material is in mass production and commercially available in a variety of shapes, sizes and trademarks. It is used in form of ceramics since 1960s (Jaffe et al., 1971) and recently in form of thin films (Shur et al., 1997, Kuznetsov et al., 2006).

The parameters of PZT 52/48 are as follows: the density is $7.5 \cdot 10^3$ kg/m^3, the dielectric constant is $\varepsilon = 1300$, the Curie temperature is 593 K, the Young's modulus is $7.8 \cdot 10^{10}$ N/m^2, the piezoelectric constant is $d_{33} = 295 \cdot 10^{-12}$ C/N, and the piezoelectric constant is $g_{33} = 25 \cdot 10^{-3}$ m^2/C (Online B).

FEG ferroelectric elements investigated in (Shkuratov et al., 2004; Shkuratov et al., 2006a; Shkuratov et al., 2006c; Shkuratov et al., 2007a; Shkuratov et al., 2007b; Shkuratov et al., 2007c; Shkuratov et al., 2008a; Shkuratov et al., 2008b) were PZT 52/48 disks polarized along the cylindrical axis. Silver contact plates (electrodes) were deposited on both ends of the PZT disks by electron beam deposition, and each disk was poled by the manufacturer to its remnant polarization value. The diameters of the ferroelectric disks were 25.0, 25.4, 26.1, and 27.0 mm, and their thicknesses varied from 0.65 mm to 6.5 mm (Table 1).

Diameter, D (mm)	Thickness, h (mm)
26.1	0.65
27.0	2.10
25.0	2.50
25.4	5.10
25.0	6.50

Table 1. Sizes of investigated PZT 52/48 ferroelectric elements of the FEGs.

To investigate FEG pulsed power generation in the high-resistance mode, we used a Tektronix P6015A high-voltage probe as a load. The impedance of the probe was 10^8 Ω and its capacitance was 3 pF, so the current in the electrical circuit of the FEG was negligible (less than $5 \cdot 10^{-4}$ A at 50 kV output voltage).

The experimental setup and circuit diagram of the system for investigation of the operation of the FEG in the high resistance mode are shown in Fig. 3. The high-voltage output

terminal of the FEG (positive plate of the ferroelectric element) was connected directly to the high-voltage probe, and the negative (front) plate of the PZT disk was grounded. Note that high-voltage diodes or high-voltage rectifiers were not used in these experiments.

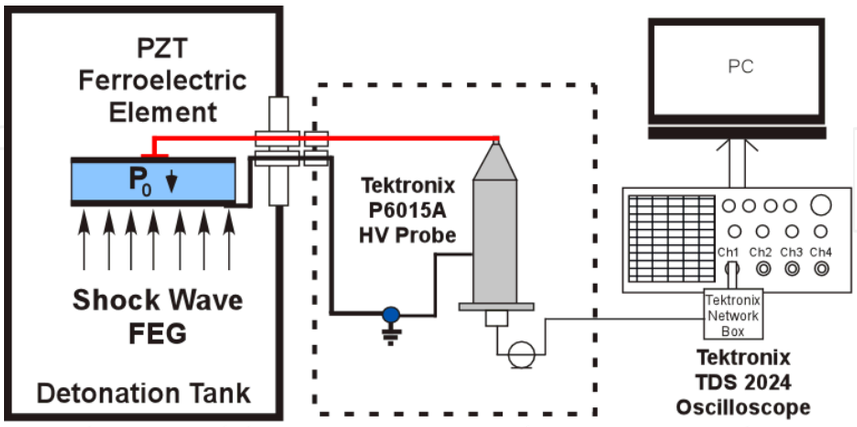

Fig. 3. Schematic diagrams of the measuring system for investigating the operation of FEG in the high-resistance mode.

The operation of the FEG was as following. After detonation of high explosives, an accelerated flyer plate impacted the ferroelectric element and initiated a shock wave. The shock wave propagated through the ferroelectric element and depolarized it. The depolarization process released the induced electric charge on the metallic contact plates of the ferroelectric element and a voltage pulse (electromotive force pulse) appeared on the output terminals of the generator.

The waveform of a typical electromotive force (e.m.f.) pulse produced by an FEG containing a PZT 52/48 ferroelectric element of D = 25.0 mm/h = 6.5 mm is shown in Fig. 4. The amplitude of the e.m.f. pulse reached $E_g(t)_{\max}$ = 21.4 kV and the full width at the half maximum (FWHM) was 1.1 μs.

In Fig. 4, the increase in the e.m.f. pulse from zero to its peak value is the direct result of the depolarization of the ferroelectric element due to explosive detonation shock wave action. Shock wave depolarization induced an electric charge that was released at the contact plates of the ferroelectric disk. Because of the high resistance and low capacitance of the load in this mode of operation, the released electric charge was charging the ferroelectric element (it is initially a capacitor) to a high voltage. The rise-time of the e.m.f. pulse is related to the shock front propagation time through the ferroelectric disk thickness.

Since there was no electric charge transfer from the ferroelectric element to the external circuit in this mode of operation of the FEG (Fig. 3), one might expect that the waveform of the e.m.f. produced by the FEG would be a square pulse of $E_g(t)_{\max}$ amplitude, with a flat top and lasting several or more microseconds (until the mechanical destruction of the ferroelectric element occurred). It follows from the experiments, however, that after reaching its maximum value the e.m.f. pulse does not hold its maximum value, but decreases rapidly (see Fig. 4).

To understand this phenomenon it is necessary to take into a consideration that the shock wave propagating through the ferroelectric element had very complex characteristics (Reynolds & Seay, 1961; Reynolds & Seay, 1962; Halpin, 1966; Setchell, 2003). The shock

represents the superposition of a number of elastic and inelastic acoustic and shock waves (Setchell, 2003) that depolarize the ferroelectric element and simultaneously change its physical properties significantly. Apparently, the rapid decrease of the e.m.f. pulse after it reached its peak value, $E_g(t)_{max}$, was the result of a significant increase in the electrical conductivity of the shock-compressed ceramic material (behind the shock as it traveled through the disk) and a corresponding leakage current in the element, or of internal electrical breakdown within the ceramic disk.

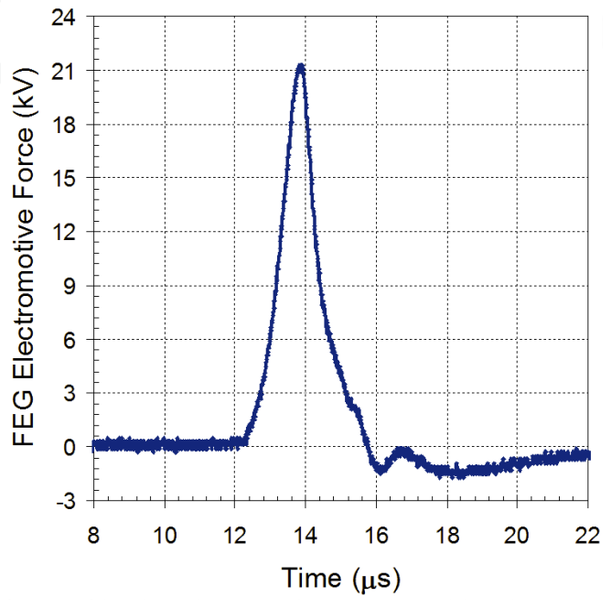

Fig. 4. A typical waveform of high voltage pulse produced by the FEG containing PZT 52/48 element with D = 25.0 mm/h = 6.5 mm.

In spite of complex and not completely understood physical processes in shocked ferroelectrics, we have found out that there are two linear relationships between PZT 52/48 element thickness and parameters of the high voltage pulse produced by the FEG. They are presented in Figure 5.

The first linear relationship is between PZT element thickness, h, and the amplitude of the e.m.f pulse, $E_g(t)_{max}$. The second linear relationship is between h and FWHM of the e.m.f. pulse. The experiments documented in Fig. 5 show that the e.m.f. pulse amplitude and FWHM are highly reproducible. An increase in PZT 52/48 element thickness leads to an increase of both the e.m.f. pulse amplitude, $E_g(t)_{max}$, and the pulse width.

For a PZT 52/48 ferroelectric element with h = 0.65 mm, $E_g(t)_{max}$ = 3.6 ± 0.23 kV with FWHM of 0.2 ± 0.04 μs. An increase in the ferroelectric element thickness to 2.5 mm almost triples the e.m.f. pulse amplitude, to 8.9 ± 0.07 kV. The FWHM increases more than 3 times to 0.62 ± 0.02 μs. For a ferroelectric element having h = 5.1 mm, $E_g(t)_{max}$ = 17.03 ± 0.25 kV with a FWHM of 0.9 ± 0.03 μs.

It follows from the experimental data shown in Fig. 5 that the amplitude of the e.m.f. pulse is directly proportional to the PZT 52/48 element thickness, with a coefficient of proportionality equal to 3.4 ± 0.5 kV/mm. Apparently, this electric field strength (3.4 kV/mm) is the internal electrical breakdown field for PZT 52/48 ferroelectric material. The

FWHM is directly proportional to the thickness of the PZT 52/48 ferroelectric element, with a coefficient of proportionality equal to 0.21 ± 0.02 μs/mm.
Therefore, we experimentally demonstrated that miniature explosively driven ferroelectric generators are capable of producing high-voltage pulses of several tens of kilovolts for a few microseconds in a high-resistance load.

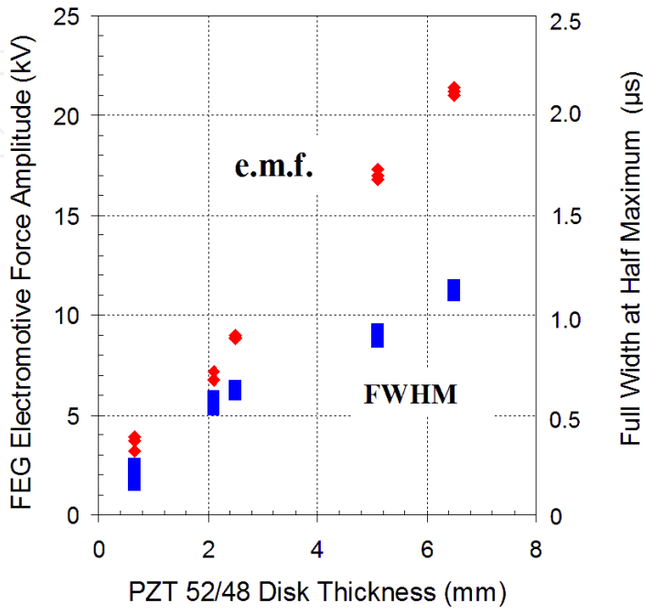

Fig. 5. From (Shkuratov et al., 2004; Shkuratov et al., 2006a; Shkuratov et al., 2006c; Shkuratov et al., 2007a; Shkuratov et al., 2008a; Shkuratov et al., 2008b): experimentally obtained dependence of e.m.f. pulse amplitudes (diamonds) and FWHM (squares) produced by FEGs versus thicknesses of PZT 52/48 ferroelectric elements.

4. Depolarization of PZT 52/48: Longitudinal Explosive Shock Versus Quasi-Static Thermal Heating

The quantity of electric charge released in the electrical circuit of an FEG during its explosive operation determines the amount of electrical energy produced by the generator in its load circuit. Therefore, the efficiency of the device depends on the degree of the depolarization of the ferroelectric element under the action of a shock wave. In this section, we describe the results of comparative systematic studies of the depolarization of PZT 52/48 ceramic by means of two techniques – thermal heating, and longitudinal compression by shock waves from the detonation of an explosive charge.
A schematic diagram of the experimental setup we developed for thermal depolarization of ferroelectric samples is shown in Fig. 6 (Shkuratov et al., 2010). In this setup, we used an automatically controlled Thermolyne 47900 furnace, and during each experiment placed a ferroelectric sample in a thermal bath (a beaker filled with ultra-fine sand) close to a K-type thermocouple. We connected the thermocouple to a SPER Scientific thermometer (Model 800005), and the signal cables from the ferroelectric sample to a Keithly 2400 pico-ampere meter.

The heating rate did not did not exceed 1 K/min for all studied samples. Detailed description of technique of thermal depolarization experiments is given in (Shkuratov et al., 2010).

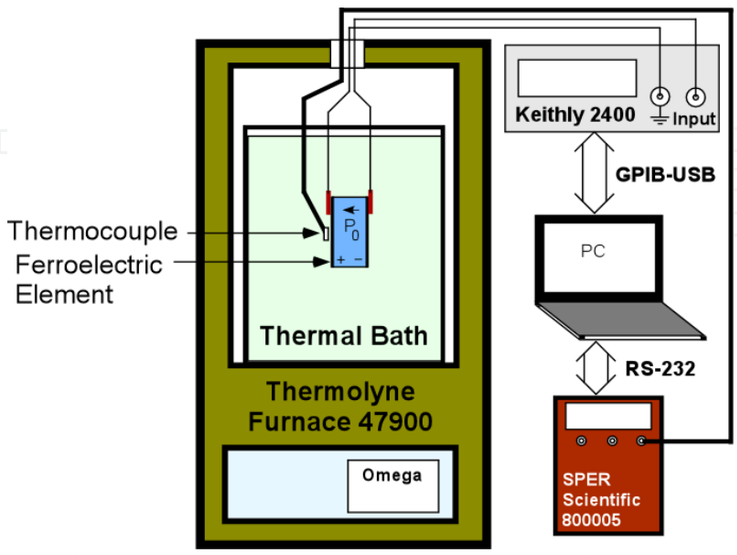

Fig. 6. A schematic diagram of the experimental setup used for measurement of thermal depolarization of ferroelectric samples.

A diagram of the measuring circuit we developed for explosive shock depolarization experiments is shown in Fig. 7 (Shkuratov et al., 2006c; Shkuratov et al., 2007b; Shkuratov et al., 2010). A schematic of shock wave FEG used in these experiments is shown in Fig. 1. The load loop (Fig. 7) was made of a copper strip 12.0 mm wide and 1.0 mm thick. The load loop (Fig. 7) resistance and inductance were R_L(100 kHz) = 0.57 Ω and L_L(100 kHz) = 0.98 μH, respectively.

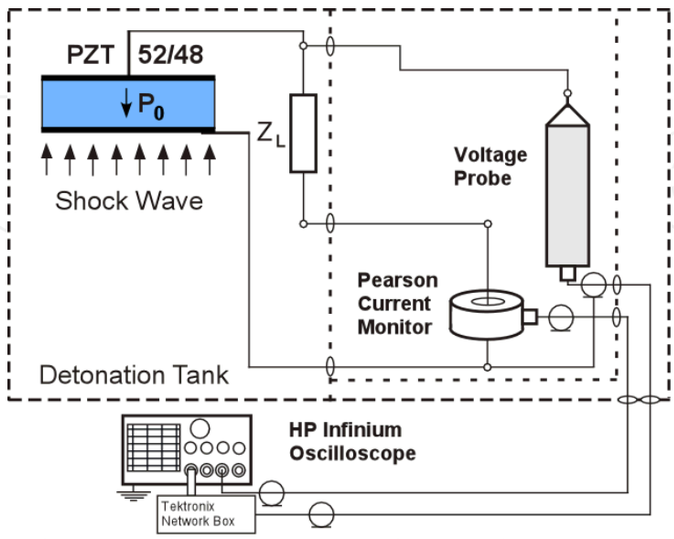

Fig. 7. A schematic diagram of the experimental setup for investigation of longitudinal shock depolarization of the PZT 52/48 ceramic samples.

Typical plots of the thermally induced current, I_h(T), for PZT 52/48 ceramic disk of 26.1 mm diameter are shown in Fig. 8. The I_h(T) is not a monotonic function of temperature, and it has a few well-resolved peaks. The relative amplitudes of the peaks and their positions varied with disk thickness (Shkuratov et al., 2010). Each sample we investigated, no matter the size (see Table 1), had the most pronounced peak of I_h(T) at T = 405±3 K. This temperature is in good agreement with the temperature at which the samples were poled by the manufacturer. Commercial PZT 52/48 samples are poled by ITT Corp at temperatures ranging from 400 K to 410 K (Online B). Heating the ferroelectric samples higher than 420 K can lead to an increase in leakage currents to a level that could result in thermal runaway and electrical breakdown during the poling procedure (Moulson & Herbert, 2003).

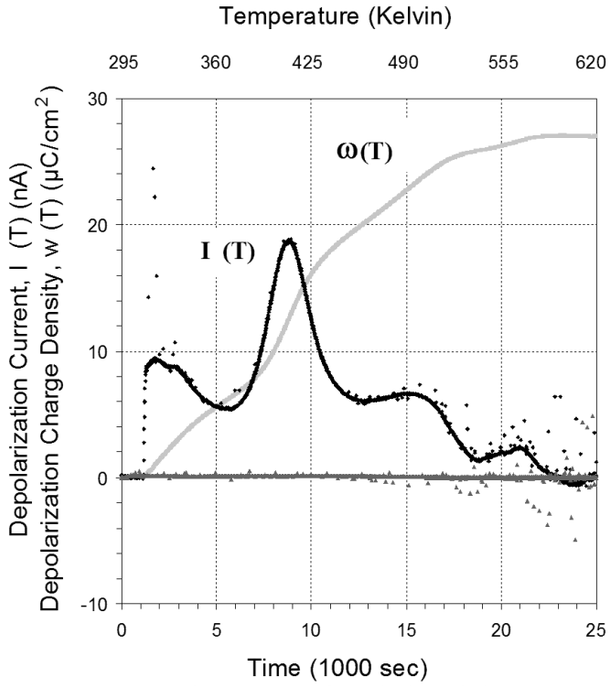

Fig. 8. Typical depolarization curve for PZT 52/48 disks of diameter D = 26.1 mm/ thickness h = 0.65 mm. Initial depolarization current (first heating cycle) is black curve. The electric charge released in the circuit is light gray curve. Second heating cycle depolarization current is dark gray curve.

It follows from our experimental results that a second heating cycle of the PZT 52/48 samples caused no current flow in the circuit (Fig. 8). In this case, the current recorded from each investigated sample was practically zero.

This is direct experimental evidence that during the first heating cycle (Fig. 8), PZT 52/48 undergoes a structural phase transition into the cubic phase on the PZT composition-temperature phase diagram (Jaffe et al., 1971). The samples are completely depolarized during the first heating cycle, and all compensating electric charge density stored in the samples' electrodes is released to the external circuit.

The depolarization charge density, ω, is the integral of the experimentally measured depolarization current divided by the electrode area, A

$$\omega(T(t)) = \frac{1}{A} \cdot \int_0^{t_F} I_h(T(t)) \cdot dt \tag{1}$$

where t_F is the time of the depolarization process. The experimental data for all sample sizes we studied are summarized in Table II. The thermally-induced depolarization charge density was consistent for all sample sizes, $\omega = 27.7\ \mu C/cm^2$.

The flyer plate of the FEG longitudinally impacted the ferroelectric body so that the shock wave traveled in a direction parallel to the ferroelectric polarization vector $\boldsymbol{P_0}$ (Fig. 7). Prior to the flyer plate impact, the electric field in the ferroelectric sample was equal to zero because the surface charge density (the bonded charge) compensated the polarization of the sample, $\boldsymbol{P_0}$, that was obtained during the poling procedure. When a shock wave depolarized a ferroelectric disk, a pulsed e.m.f. appeared on the metallic electrodes of the ferroelectric element. When the electrical circuit of the generator was closed (a load is connected to the output terminals of the FEG) the e.m.f. caused a pulsed electric current, $I(t)$, in the circuit. Integration of the $I(t)$ waveform from 0 to t gives the momentary value of the electric charge, $\Delta Q(t)$, released to the electrical circuit due to depolarization of the PZT

$$\Delta Q(t) = \int_0^{t_F} I(t) \cdot dt \tag{2}$$

It should be noted that t_F in the shock experiments ranges from 10^{-6} to 10^{-5} s. It is about 9-10 orders of magnitude lower than t_F in the thermal depolarization experiments (the time for the thermally induced charge to be released).

Typical waveforms of the shock induced depolarization current produced by a PZT 52/48 disk of D = 26.1 mm / h = 0.65 mm, and the electric charge released from the sample are presented in Fig. 9.

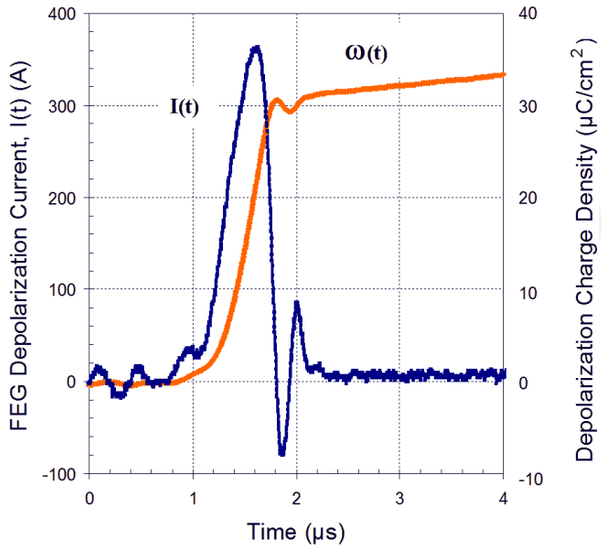

Fig. 9. Waveform of the pulsed depolarization current, $I(t)$, and the depolarization charge density, $\omega(t)$, released due to longitudinal shock compression of PZT 52/48 disk with D = 26.1 mm / h = 0.65 mm.

The peak depolarization current generated by longitudinally-shock-compressed PZT element was $I(t)_{max}$ = 360 A, with FWHM of 0.5 μs. The electric charge density released from the sample due to the shock compression was ω = 30.6 μC/cm². The depolarization charge density for all PZT 52/48 samples we investigated are presented in Table 2.

Diameter of the PZT 52/48 disks (mm)	26.1	27.0	25.4
Thickness of the PZT 52/48 disks (mm)	0.65	2.1	5.1
Thermal depolarization charge density (μC/cm²)	27.9±1.8	27.8±1.5	27.9±1.6
Adiabatic (shock induced) high-pressure depolarization charge density (μC/cm²)	29.7±2.4	27.5±2.2	26.7±2.2

Table 2. Sizes of PZT 52/48 disks and electric charge released by disks due to thermal depolarization and adiabatic (longitudinal-shock-wave) high-pressure depolarization.

It follows from our experimental results (Shkuratov et al., 2010) that increasing the thickness of the PZT disk led to decreased shock depolarization current amplitude, and increased current pulse FWHM. The latter is apparently the result of the longer shock wave front propagation time in the thicker samples. Figure 10 presents the amplitude of the depolarization current generated by longitudinally-shock-compressed PZT 52/48 disks, versus the thickness of the disks. It follows from our experimental results that the current amplitude is inversely proportional to the disk thickness.

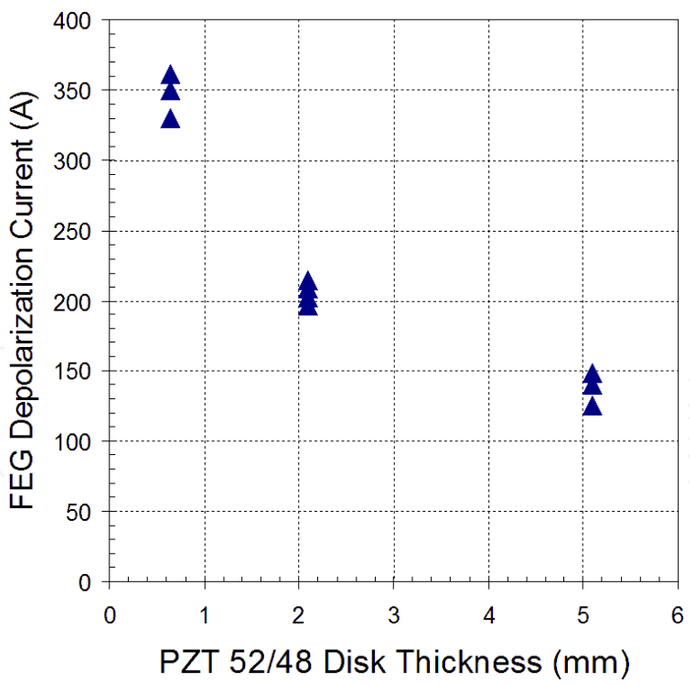

Fig. 10. Amplitude of shock induced depolarization current versus thickness of PZT 52/48 disks.

Experimental data for both the thermal and adiabatic (shock-induced) depolarization of all PZT 52/48 samples we studied are shown in Fig. 11. The shock pressure in the bulk PZT 52/48 ceramic elements was determined in (Shkuratov et al., 2010), P_{SW} = 1.5 ± 0.2 GPa.

It is clear from results presented in Fig. 11 that the depolarization charge released due to longitudinal shock wave compression of PZT 52/48 disks is almost equal than that released due to thermal heating. This is direct evidence of almost complete depolarization of the PZT 52/48 elements due to their compression by longitudinal shock waves within the FEGs.

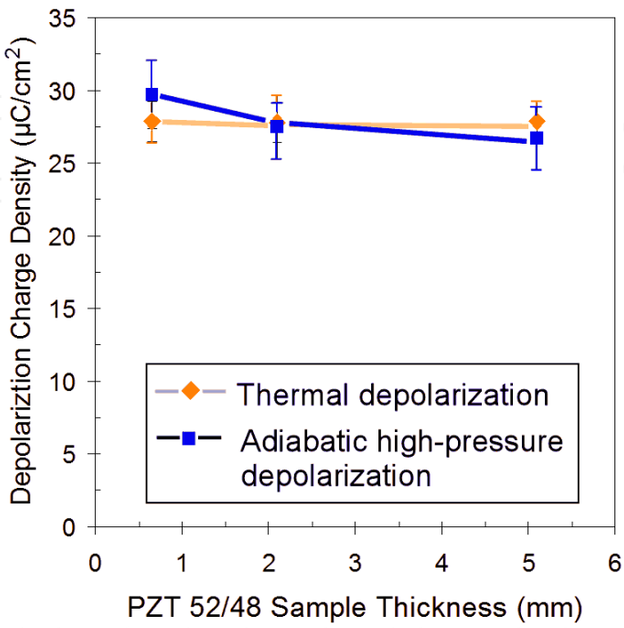

Fig. 11. Experimental data for the thermal and longitudinal explosive shock wave depolarization of PZT 52/48 samples.

It follows from the results we obtained (Fig. 11) that despite the small size of ferroelectric generators and their correspondingly imperfectly-shaped shock wave fronts, these devices provide almost complete shock-wave depolarization of the PZT 52/48 ferroceramic elements.

One of the effects we observed was a monotonic decrease of the electric charge released from shock-compressed PZT 52/48 samples with increasing sample thickness (Fig. 11). A possible explanation of this effect can be based on the shock wave splitting phenomena observed earlier by Reynolds and Seay (Reynolds & Seay, 1961; Reynolds & Seay, 1962). They showed that a longitudinal shock wave in PZT 52/48 splits into two shock waves; the split shocks result in decreased depolarization charge. It is possible that such shock splitting has only a minor effect in thin samples. An increase of the thickness of the samples leads to an increase in shock wave travel distance, and to a more significant separation of the shock waves. Other possibilities may include the dispersion of the shock as it crushes the sample while transiting the its length, or shock attenuation as the rarefaction(s) behind the shock catch(es) the shock, or some combination of these processes.

In Section 3 of this Chapter we have demonstrated that the output voltage produced by the FEG is directly proportional to the thickness of PZT 52/48 element up to h = 6.5 mm. The effect of reduction of the electric charge transfer from longitudinally-shock-compressed PZT 52/48 elements with increasing the element's thickness we detected may pose a problem in the development of FEGs utilizing ferroelectric elements thicker than 10 mm for producing ultrahigh output voltage.

5. Pulse Charging of Capacitor Bank by Explosively Driven FEG

Various types of pulsed power systems built around capacitive energy storage devices are widely used in modern technology for production of charged-particle beams, generation of pulsed high power microwaves and others pulsed power technologies (Mesyats, 2005). In these generators, electric energy is provided to the capacitive energy storage from high-voltage power sources powered from a conventional 110/220 V - 50/60 Hz supply line. The operation theory of these generators is well-developed (Mesyats, 2005).
However, certain special applications require that the pulsed power system be autonomous. Another necessary condition is compactness of the device as a whole. We proposed and experimentally studied an autonomous two-stage pulsed power system based on a shock-wave ferroelectric generator as a charging source for a capacitive energy storage (Shkuratov et al., 2007c; Shkuratov et al., 2007d; Shkuratov et al., 2008a; Shkuratov et al., 2008b). We have experimentally demonstrated that a miniature explosively driven FEG can successfully charge capacitor banks of different capacitances. We have developed a model and made a successful digital simulation of the operation of the FEG-Capacitor bank system. We present some results of these studies in this section.

5.1. FEG-Capacitor Bank System

A diagram of the experimental setup we developed for investigations of the FEG-Capacitor bank system is shown in Fig. 12 (Shkuratov et al., 2008a; Shkuratov et al., 2008b).

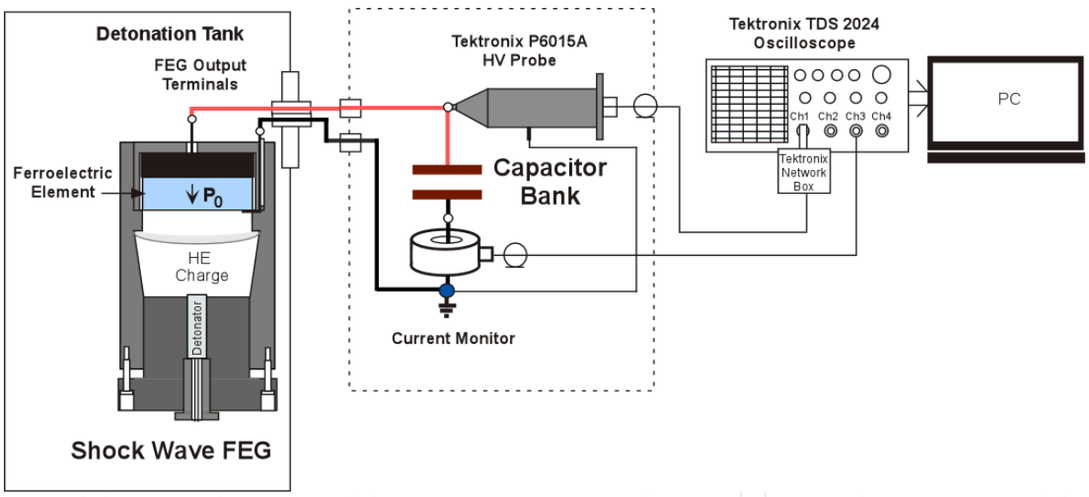

Fig. 12. Schematic diagrams of the measuring system for investigating the operation of the FEG-Capacitor bank system.

The high voltage output of the FEG was connected to the high-voltage terminal of the capacitor bank and to the Tektronix P6015A high-voltage probe (Fig. 12). The negative plate of PZT disk was connected to the ground terminal of the capacitor bank through a commercial current monitor. We did not use high-voltage diodes or rectifiers in these experiments.
The first series of FEG-Capacitor bank experiments was performed with PZT 52/48 elements having diameter D = 26.1 mm and thickness h = 0.65 mm. The capacitance of the capacitor

bank was C_L = 18 nF. It is more than two times higher than initial capacitance of the FEG, C_G = 7.1 ± 0.1 nF.

Figure 13(A) shows a typical waveform of the high voltage produced by an FEG across an 18 nF capacitor bank. It is not a single pulse, but a series of oscillations. The frequency of oscillations is about 1.0 MHz. The peak voltage amplitude of the first pulse was $U(t)_{max}$ = 2.16 kV, the FWHM of the first pulse was 0.54 μs, and τ = 0.34 μs.

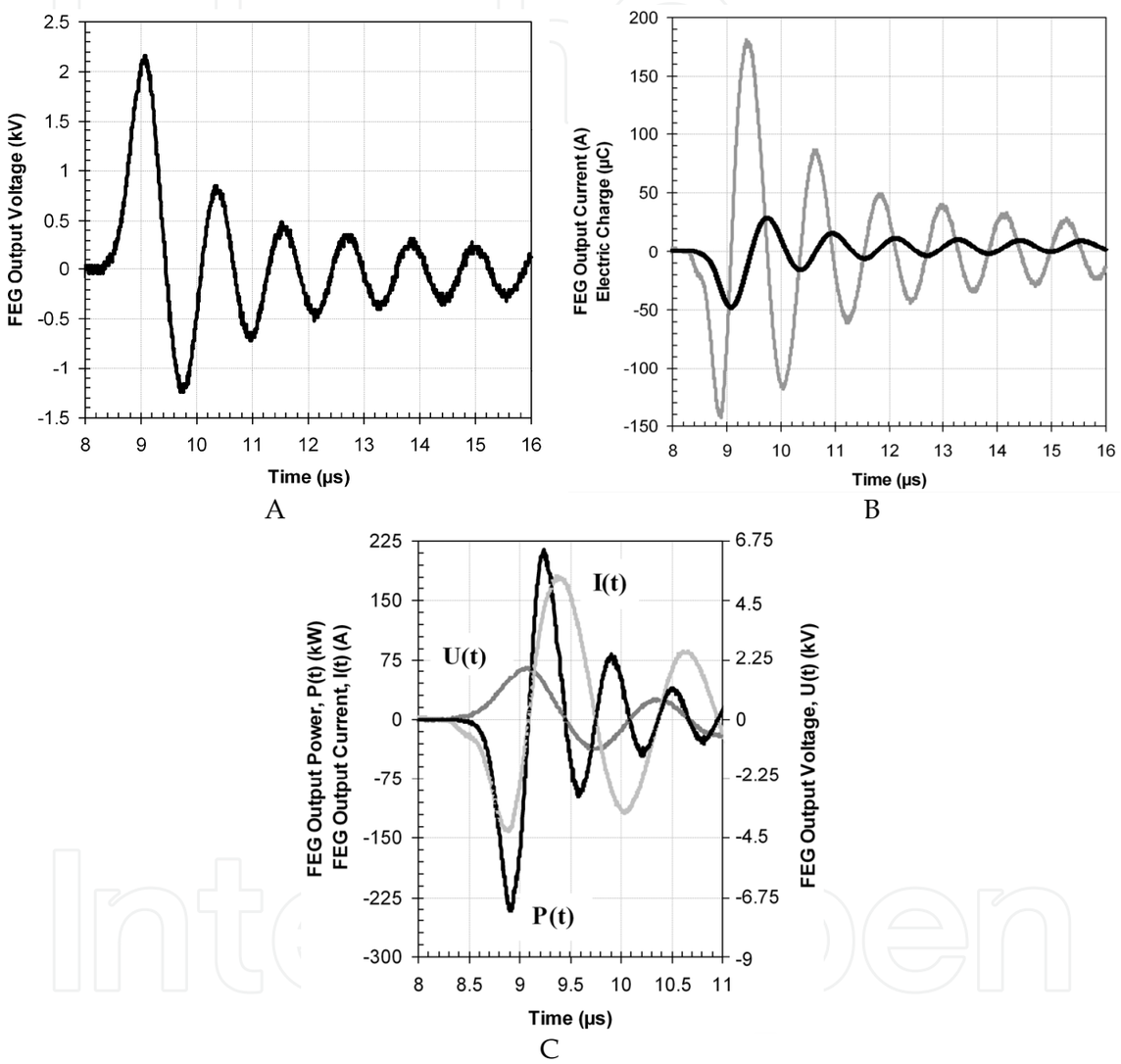

Fig. 13. A – waveform of the output voltage; B – waveform of current (gray) and circulation of electric charge (black); C – waveforms of voltage (dark gray), current (light gray) and power (black) produced by the FEG. PZT 52/48 disk with D = 26.1 mm / h = 0.65 mm. 18 nF capacitor bank.

The peak energy delivered to the capacitor bank in this experiment [the first pulse in Fig. 13(A)] reached $W(t)_{max} = C_0\ U(t)_{max}^2/2$ = 42 mJ. The average amplitude of the first high voltage pulse produced by the FEG across the capacitor bank in this series of experiments

was $U(t)_{max\ ave}$ = 2.07 ± 0.22 kV. The average peak energy delivered to an 18 nF capacitor bank reached $W(t)_{max\ ave}$ = 39 ± 0.4 mJ.

Figure 13(B) shows the waveform of the charging current, $I(t)$, produced by the FEG in the circuit and circulation of electric charge. The peak amplitude of the first current pulse was $I_1(t)_{max}$ = 140 A, the FWHM was 0.3 μs and the rise-time τ = 0.52 μs. The peak amplitude of the second current pulse was higher than the first one and reached $I_2(t)_{max}$ = 180 A, with FWHM = 0.45 μs and τ = 0.31 μs. Integration of the charging current, $I(t)$, waveform from 0 to t gives the momentary value of the electric charge, ΔQ(t), transferred to the external electrical circuit during explosive operation of the FEG (Eqn. 2).

As it follows from the experiment [Fig. 13(B)], the electric charge transferred from a PZT module during explosive operation of the FEG to the capacitor bank, ΔQ_{max} = 50 μC, is 33.3% of the initial charge stored in the ferroelectric element due to its remnant polarization, Q_0 = 150 μC (see Table 2 in Section 4 of this Chapter).

Waveforms of the output high voltage $U(t)$, current $I(t)$, and power $P(t)$ pulses produced by an FEG across 18 nF capacitor bank are shown in Fig. 13(C). The power dissipated in the load, $P(t)$ was determined as the product of the instantaneous value of the output voltage $U(t)$ by the instantaneous current in the circuit, $I(t)$: $P(t) = I(t) \cdot U(t)$. The peak output power reached $P(t)_{max}$ = 0.24 MW.

It should be noted that peak power produced by the FEG is 5 to 7 times higher than that produced by recently developed miniature prime power sources based on shock wave demagnetization of $Nd_2Fe_{14}B$ ferromagnets, shock wave ferromagnetic generators (FMGs) (Shkuratov et al., 2002a; Shkuratov et al., 2002b; Shkuratov et al., 2002c; Shkuratov et al., 2003a; Shkuratov et al., 2003b; Shkuratov et al., 2006b). At the same time the FMG produces much longer power pulse than the FEG (FWHM = 0.3 μs for FEG and FWHM = 8.0 μs for FMG).

The next series of experiments was performed with double less capacitance of the bank C_L = 9 nF. The output voltage oscillated as it did in the experiments with an 18 nF capacitor bank (Fig. 13). The frequency of oscillations was slightly higher, ~ 1.1-1.2 MHz in compare with C_L = 18 nF. The average amplitude of the first high voltage pulse produced by the FEG across a 9 nF capacitor bank was $U(t)_{max\ ave}$ = 2.41 ± 0.33 kV. The average peak energy delivered to a 9 nF capacitor bank reached $W(t)_{max\ ave}$ = 26 ± 0.5 mJ.

It follows from experiments with 9 nF and 18 nF capacitor banks that increasing the capacitor bank capacitance leads to increasing the energy transferred from the PZT module to the capacitor bank. This result was confirmed in the third series of FEG-Capacitor bank experiments.

The third series of experiments was performed with capacitance of the bank C_L = 36 nF. Figure 14(A) shows a typical waveform of the high voltage produced by an FEG across a 36 nF capacitor bank. Results of these experiments were different from the results obtained with the 18 nF and 9 nF capacitor banks. The FEG produced a series of oscillations, but the amplitude of the first half-wave is significantly higher than the next one. Oscillations were damping quickly. Amplitude of the first half-wave of output voltage was $U(t)_{max}$ = 1.82 kV with FWHM = 0.85 μs, and τ = 0.93 μs.

The energy delivered to a 36 nF capacitor bank was $W(t)_{max}$ = 60 mJ and the specific energy density of the PZT element was 171 mJ/cm^3. The average amplitude of the first half-wave of high voltage across a 36 nF capacitor bank was $U(t)_{max\ ave}$ = 1.75 ± 0.14 kV.

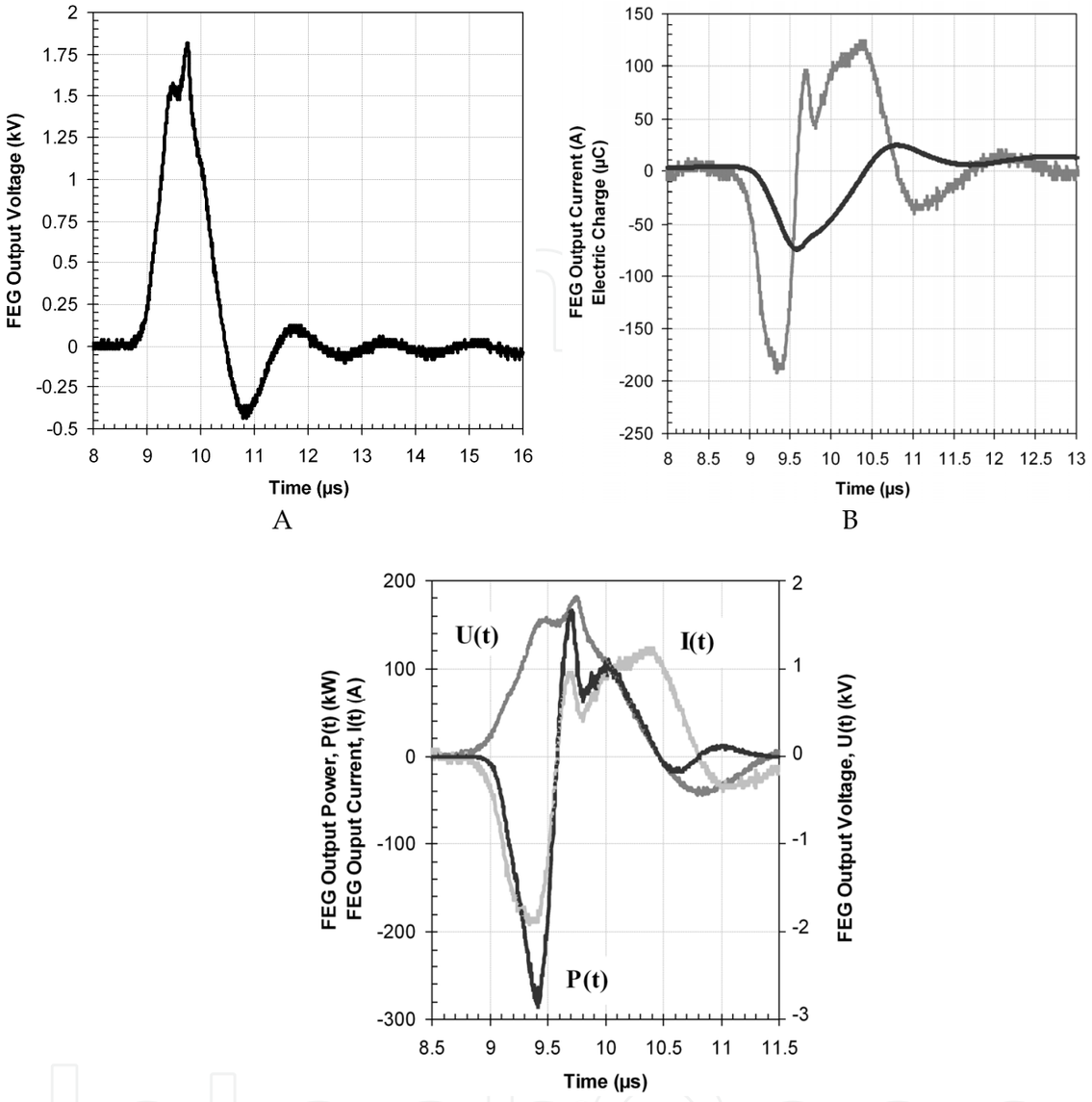

Fig. 14. A – waveform of the output voltage; B – waveform of current (gray) and circulation of electric charge (black); C – waveforms of voltage (dark gray), current (light gray) and power (black) produced by the FEG. PZT 52/48 disk with D = 26.2 mm/h = 0.65 mm. 36 nF capacitor bank.

The average peak energy delivered to a 36 nF capacitor bank reached $W(t)_{\max\ ave}$ = 55 ± 0.3 mJ. Fig. 14(B) shows the waveform of the output current, $I(t)$, produced by the FEG in the circuit and circulation of electric charge. The total charge delivered from the PZT energy-carrying element to the 36 nF capacitor bank in this experiment was ΔQ_{max} = 73 μC, which is 49% of the initial charge.

The peak power produced by the FEG was $P(t)_{max}$ = 0.29 MW (Fig. 14). It is about 8 times higher than that produced by miniature FMG charging the same capacitor bank (Shkuratov et al., 2006a). Table 3 summarizes results of FEG-Capacitor bank experiments for all three

capacitance of the bank. It follows from our experimental results that the capacitance of the capacitor bank effects significantly on the character of processes in the FEG-Capacitor bank circuit.

Capacitance (nF)	Voltage Amplitude (kV)	Transferred Energy (mJ)
9 nF	2.41 ± 0.33 kV	26 ± 0.5
18 nF	2.07 ± 0.22 kV	39 ± 0.4
36 nF	1.75 ± 0.14 kV	55 ± 0.3

Table 3. Amplitude of maximum output voltage, $U(t)_{max}$, generated in FEG-Capacitor bank system and energy transferred from the FEG module to the capacitor bank as a function of capacitance of the bank. PZT 52/48 elements with diameter D = 26.1 mm and thickness h = 0.65 mm.

We performed systematic experimental studies of FEG-Capacitor bank systems with FEGs containing PZT 52/48 elements of different sizes (Shkuratov et al., 2007c; Shkuratov et al., 2008a; Shkuratov et al., 2008b). Figure 15(A) summarizes experimentally obtained high-voltage pulse amplitudes produced by FEGs of three types versus the capacitance of the capacitor bank.

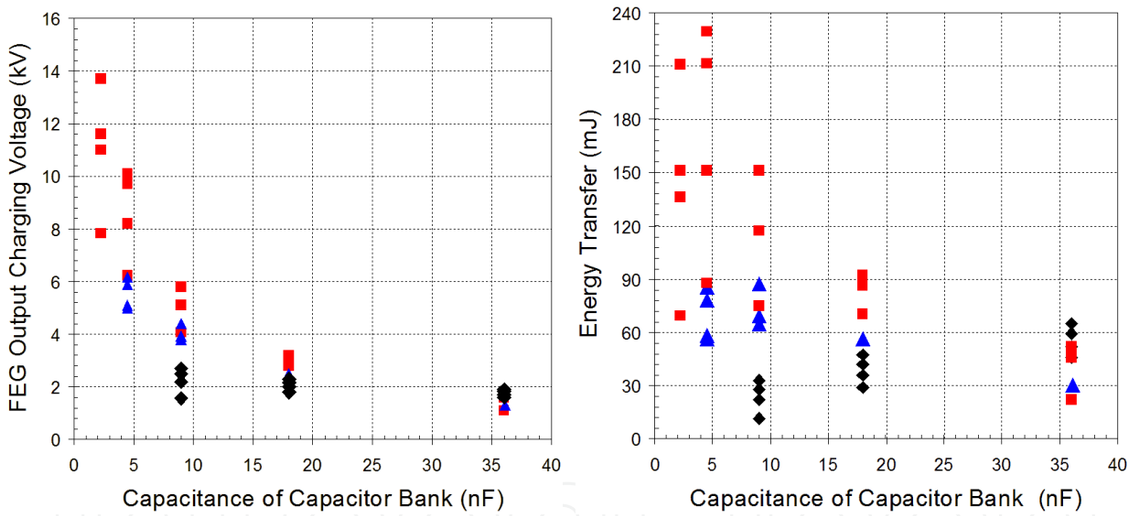

A B

Fig. 15. Performance of FEG-Capacitor bank system. A - amplitude of the voltage pulse produced by FEGs across capacitor banks of different capacitance. B - energy delivered from FEGs to capacitor banks of different capacitance. PZT 52/48 elements of D = 26.1 mm/h = 0.65 mm (diamonds), D = 27.0 mm/h = 2.1 mm (triangles) and D = 25.4 mm/h = 5.1 mm (squares).

It follows from the experimental results that increasing the capacitance of the bank leads to a gradual decrease in the high-voltage produced by the FEGs containing all three types of PZT 52/48 ferroelectric elements (D = 26.1 mm/h = 0.65 mm, D = 27.0 mm/h = 2.1 mm and D = 25.4 mm/h = 5.1 mm).

The highest voltage, $U_{\text{charge max}}$ = 13.7 kV, was obtained across a 2.25 nF capacitor bank from the FEG containing PZT element of D = 25.4 mm/h = 5.1 mm. The lowest voltage, $U_{\text{charge min}}$ = 1.2 kV, was obtained across a 36 nF capacitor bank from the same type of FEG [Fig. 15(A)]. Figure 15(B) summarizes experimental results obtained in (Shkuratov et al., 2007c; Shkuratov et al., 2008a; Shkuratov et al., 2008b) for the energy delivered from FEGs to capacitor banks of different capacitances. It can be clearly seen the maximum energy transfer from the FEG containing PZT 52/48 elements of D = 25.4 mm/h = 5.1 mm to the capacitor bank at bank capacitance of 4.5 nF [Fig. 15(B)]. Increasing the capacitance of the bank from 4.5 to 36 nF results in significant decreases in the energy transfer from 177±27 mJ to 47±12 mJ. Decreasing the capacitance from 4.5 to 2.25 nF leads to a decrease in the energy transferred to 156±25 mJ.
A similar effect was observed with FEGs containing PZT 52/48 elements of D = 27.0 mm/h = 2.1 mm [Fig. 15(B)]. In that case, the maximum energy transfer took place with capacitance of the bank of 9 nF.

5.2. Theoretical Model of FEG-Capacitor Bank System

To explain oscillatory behavior of output signals produced in the FEG-Capacitor bank system (Fig. 13) we developed a computer model of the system (Shkuratov et al., 2007d; Shkuratov et al., 2008a). A schematic diagram illustrating the depolarization of a ferroelectric module under longitudinal shock wave impact is shown in Fig. 16.

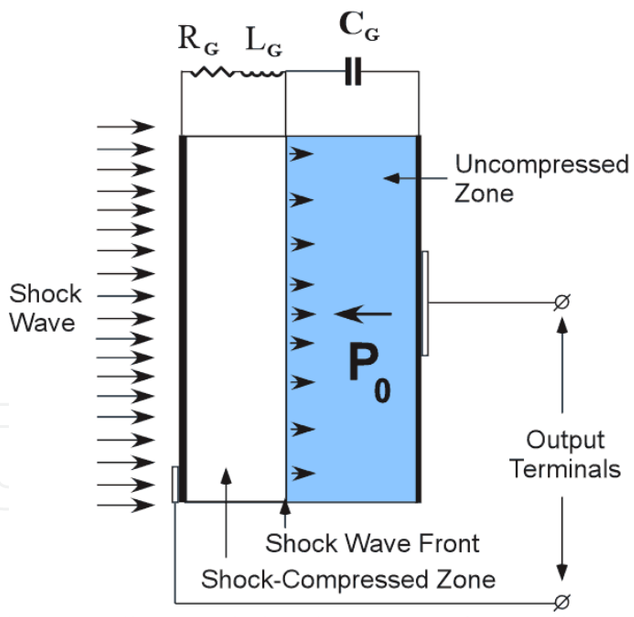

Fig. 16. Schematic diagram illustrated depolarization of PZT element under longitudinal shock wave impact.

When longitudinal shock wave passes through the polled ferroelectric element, its volume is divided into two parts or two zones, the shock-compressed zone (through which the shock wave has already passed), and the uncompressed zone (through which the shock wave has not passed). The difference in these two zones is in the value of polarization (the

compressed zone is depolarized), electrical conductivity and other physical properties (Reynolds & Seay, 1961; Reynolds & Seay, 1962; Halpin, 1966; Setchell, 2003).
The equivalent circuit of the FEG-Capacitor bank system we employed in the simulation is shown in Fig. 17 (Shkuratov et al., 2008a). The shock-compressed part of the ferroelectric element is represented in the equivalent circuit as inductance, L_1, and resistance, R_1.

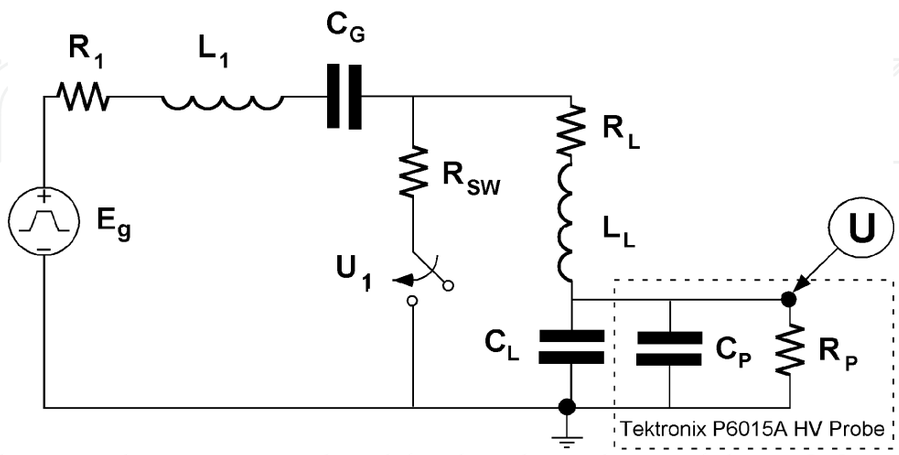

Fig. 17. The equivalent circuit employed for digital simulation of the FEG-Capacitor bank system (see the text).

The uncompressed part is represented as C_G. L_1 and R_1 are connected in series to C_G. The inductance, resistance and capacitance of the load (capacitor bank) and connecting cables are represented in the equivalent circuit as L_L, R_L, and C_L, respectively. The capacitance and resistance of Tektronix P6015A high-voltage probe are represented in the circuit as C_P = 3 pF and R_P = 100 MΩ, respectively. The internal electrical breakdown in the PZT element is simulated with switch U_1 having resistance R_{sw}. It closes when the voltage across the capacitor bank reaches the maximum value.
Result of simulation of the operation of FEG-Capacitor bank system containing PZT 52/48 element with D = 26.1 mm/h = 0.65 mm and C_L = 18 nF is shown in Fig. 18(A). The voltage across the bank oscillates as it did in the experiment (Fig. 13). The parameters of the system were as follows: C_G = 7 nF, L_1 = 5 μH, R_1 = 0.2 Ω, C_L = 18 nF, L_L = 2 μH, R_L = 2 Ω, R_{sw} = 0.3 Ω.
Result of simulation of the operation of FEG-Capacitor bank system containing PZT 52/48 element with D = 26.1 mm/h = 0.65 mm and C_L = 36 nF is shown in Fig. 18(B). The parameters of the system C_G, L_1, R_1, L_L, R_L were equal to those for the case with capacitor bank of 18 nF [Fig. 18(A)]. The different parameters in comparison with the case of 18 nF bank are: capacitance of the bank C_L = 36 nF and resistance of the PZT element after internal electrical breakdown R_{sw} = 4.3 Ω. The output voltage of the FEG is 20% lower than in case of an 18 nF bank [Fig. 18(B)] and it is practically a single pulse as it was in the experiment (Fig. 14).
Based on results of digital simulation we can make the conclusion that a key parameter responsible for the oscillatory mode of operation of FEG-Capacitor bank system is the resistance of PZT element after electrical breakdown. It means that the intensity of the internal electrical breakdown in the shock-compressed PZT module has significant effect on the processes in the FEG-Capacitor bank system.

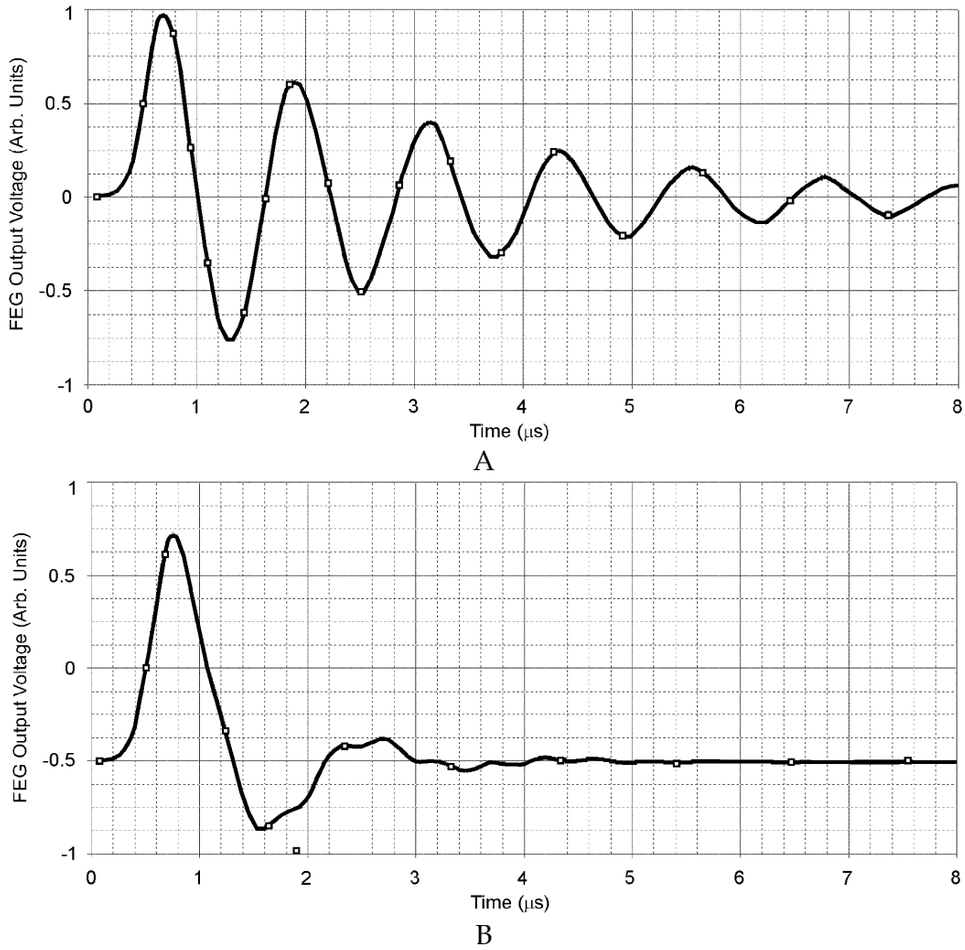

Fig. 18. Results of computer simulation of operation of FEG-Capacitor bank system.
A - capacitance of the capacitor bank of 18 nF; B - capacitance of the capacitor bank of 36 nF.

In the experiments described above, increasing the capacitance of the capacitor bank leads to decreasing the voltage produced by the FEG across the bank and, correspondingly, the voltage applied to shock-compressed ceramic disk. It effects significantly on the intensity of electrical breakdown in the shock-compressed PZT ceramics. Decreasing the voltage across the capacitor bank below threshold level results in lower impedance of conductive channels formed in the ceramics due to the electrical breakdown, and correspondingly aperiodic behavior of signals in FEG-Capacitor bank system.

6. FEG-Based Nanosecond Pulsed Power System

One of possible engineering applications of FEGs is to use it in combination with conventional pulsed power devices. A novel type of explosively driven combined pulsed power system was recently developed (Shkuratov et al., 2006a, Shkuratov et al., 2007a). The system is based on the FEG as a primary power source and the spiral vector inversion generator (VIG) as a power-conditioning stage. In this system, the amplitude of microsecond high-voltage pulses produced by FEGs can be amplified up to 20 times and the pulse width

can be compressed to the nanosecond time range. A schematic diagram of the completely explosive FEG-VIG system is shown in Fig. 19.

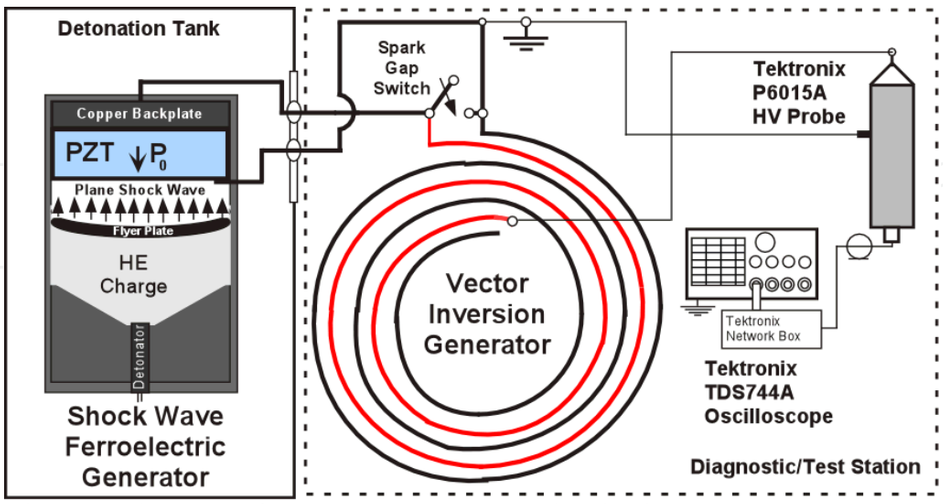

Fig. 19. Schematic diagram of a FEG-VIG nanosecond pulsed power system.

The FEG was placed inside the detonation tank. The output terminals of the FEG were connected to the input of the VIG. The negative terminal of the FEG was grounded. When fired, the FEG produced a positive high-voltage pulse that was applied to the input of the VIG spark gap switch. Detailed description of principles of operation of the FEG-VIG system is given in (Shkuratov et al., 2006a).
The waveform of a typical high-voltage pulse produced by an FEG-VIG system is shown in Fig. 20. The FEG contained PZT 52/48 disk with D = 25.4 mm/h = 5.1 mm.

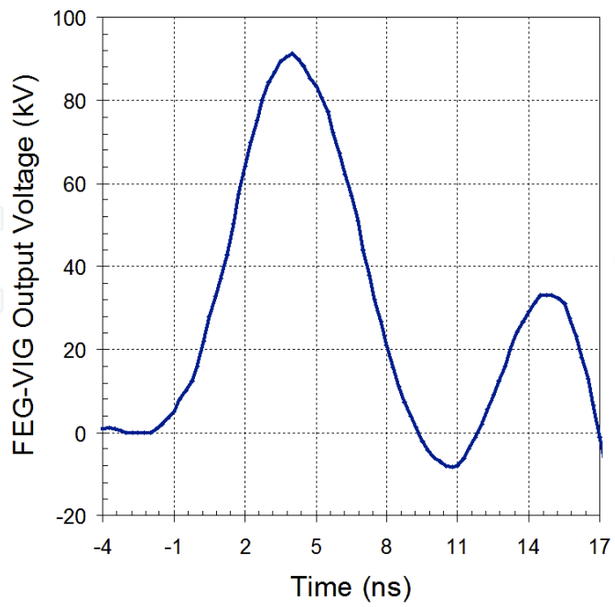

Fig. 20. Waveform of a typical high-voltage pulse produced by an explosive-driven FEG-VIG system.

This type of FEG is capable of producing output voltage up to 17 kV across the high-resistance load (see Section 3 of this Chapter). The FEG-VIG system (Figs. 19 and 20) produced high-voltage pulse with a peak voltage amplitude $U(t)_{max}$ = 91.4 kV, FWHM = 6.5 ns and τ = 5.25 ns.
Adding a VIG stage increases the voltage output of the FEG by a multiplication factor depending on the VIG's parameters, while simultaneously compressing the pulse width into the range of a few nanoseconds.

7. Summary

We designed, constructed, and systematically studied miniature explosively driven generators based on shock depolarization of polycrystalline ferroelectric elements. Results of our studies provided strong basis for understanding the operation of shock wave ferroelecric generators in different modes and its engineering applications. It was experimentally demonstrated that the amplitude of the output voltage produced by miniature FEGs across the high resistance load is directly proportional to the thickness of the ferroelectric element. The effect of almost complete shock wave depolarization of $Pb(Zr_{0.52}Ti_{0.48})O_3$ ferroelectric elements within miniature FEGs under longitudinal explosive shock pressure 1.5 GPa was detected experimentally. It was experimentally demonstrated that miniature FEGs can be used as an effective charging sources for capacitor banks. It follows from detailed parametric studies of FEG-Capacitor bank systems that there is an optimum capacitance of the bank for each type of ferroelectric element at which the maximum energy transfer is providing from the FEG to the bank. The charging power in the FEG-Capacitor bank system ranges from 0.25 to 0.30 MW. The specific energy density transferred from the PZT 52/48 element to the bank reaches 170 mJ/cm^3. It was experimentally demonstrated that the FEG-Capacitor bank system is capable of operating as a powerful oscillator with frequency up to few megahertz. Feasibility of construction of miniature autonomous 100-kV nanosecond pulsed power system based on miniature FEG and the vector inversion generator was experimentally demonstrated. Adding a VIG stage increases the voltage output of the FEG by a multiplication factor depending on the VIG's parameters, while simultaneously compressing the pulse width into the range of a few nanoseconds. This two-stage FEG-VIG pulsed power system produces an extremely high power, single-shot pulser that is unrivaled for specific power.

8. References

Altgilbers, L.L., Stults, A.H., Kristiansen, M., Neuber, A., Dickens, J., Young, A., Hold, T., Elsayed, M., Curry, R., O'Connor, K., Baird, J., Shkuratov, S., Freeman, B., Hemmert, D., Rose, F., Shotts, Z., Roberts, Z., Hackenberget, W., Alberta, E., Rader, M. & Dougherty, A. (2009). Recent advances in explosive pulsed power. *Journal of Directed Energy,* Vol. 3, No. 2, (Spring 2009) pp. 149-191.

Altgilbers, L.L., Baird, J., Freeman, B., Lynch, C.S., Shkuratov, S.I. (2010). *Explosive Pulsed Power*, Imperial College Press, ISBN 1-84816-322-3, London, U.K.

Bauer, F. & Vollrath, K. (1976a). Behaviour of non-linear ferroelectric ceramics under shock waves. *Ferroelectrics*, Vol. 12, No. 1-4, (Spring 1976) pp. 153-156, ISSN 0015-0193.

Bauer, F. & Vollrath, K. (1976b). New aspects in ferroelectric energy sources for impact fuses. *Propellants, Explosives, Pyrotechnics*, Vol. 1, No. 3, (August 1976) pp. 55-59, ISSN 0721-3115.

Cutchen, J.T. (1966). Polarity effects and charge liberation in lead zirconate titanate ceramics under high dynamic stress. *Journal of Applied Physics*, Vol. 37, No. 13, (December 1966) pp. 4745-4750, ISSN 0021-8979.

Dick, J.J. & Vorthman, J.E. (1978). Effect of electrical state on mechanical and the electrical response of a ferroelectric ceramic PZT 95/5 to impact loading. *Journal of Applied Physics*, Vol. 49, No. 4, (April 1978) pp. 2494-2498, ISSN 0021-8979.

Dungan, R.H. & Storz, L.J. (1985). Relation between chemical, mechanical, and the electrical properties of Nb_2O_5-modified 95 mol% $PbZrO_3$-5 mol% $PbTiO_3$. *Journal of the American Ceramic Society*, Vol. 68, No. 10, (October 1985) pp. 530-533, ISSN 0002-7820.

Duvall, G.E. & Graham, R.A. (1977). Phase transitions under shock-wave loading. *Reviews of Modern Physics*, Vol. 49, No. 3, (September 1977) pp. 523-579, ISSN 0034-6861.

Halpin, W.J. (1966). Currents from a shock-loaded short-circuited ferroelectric ceramic disk. *Journal of Applied Physics*, Vol. 37, No. 1, (January 1966) pp. 153-163, ISSN 0021-8979.

Halpin, W.J. (1968). Resistivity estimates for some shocked ferroelectrics. *Journal of Applied Physics*, Vol. 39, No. 8, (July 1968) pp. 3821-3826, ISSN 0021-8979.

Jaffe, B., Cook, W.R. & Jaffe, H. (1971). *Piezoelectric Ceramics*, Academic Press, ISBN 1-87890-710-7, London, U.K.

Kuznetsov, D.K., Shur, V.Ya., Baturin, I.S., Menou, N., Muller, C.H., Schneller, T., Sternberg, A. (2006). Effect of penetrating irradiation on polarization reversal in PZT thin films. *Ferroelectrics*, Vol. 340, No. 1, Part 1, (January 2006) pp. 161-167, ISSN 0015-0193.

Lysne, P.C. (1973). Dielectric breakdown of shock-loaded PZT 65/35. *Journal of Applied Physics*, Vol. 44, No. 2, (February 1973) pp. 577-582, ISSN 0021-8979.

Lysne, P.C. & Percival, C. M. (1975). The electric energy generation by shock compression of ferroelectric ceramics: Normal-mode response of PZT 95/5. *Journal of Applied Physics*, Vol. 46, No. 4, (April 1975) pp. 1519-1525, ISSN 0021-8979.

Lysne P.C. (1975). Kinetic effects in the electrical response of a shock-compressed ferroelectric ceramic. *Journal of Applied Physics*, Vol. 46, No. 9, (September 1975) pp. 4078-4079, ISSN 0021-8979.

Lysne, P.C. & Percival, C. M. (1976). Analysis of shock-wave-actuated ferroelectric power supplies. *Ferroelectrics*, Vol. 10, No. 1, (January 1976) pp. 129-133, ISSN 0015-0193.

Lysne, P.C. (1977). Resistivity of shock-wave-compressed PZT 95/5. *Journal of Applied Physics*, Vol. 48, No. 11, (November 1977) pp. 4565-4568, ISSN 0021-8979.

Mesayts, G.A. (2005). *Pulsed Power*, Kluwer Academic/Plenum Publishers, ISBN 0-306-48653-9, New York, U.S.A.

Mineev, V.N. & Ivanov, A.G. (1976). Electromotive force produced by shock compression of a substance. *Soviet Physics – USPEKHI*, Vol. 19, No. 5, (May 1976) pp. 400-419, ISSN 1063-7869.

Moulson, A.J. & Herbert, J. M. (2003). *Electroceramics: Materials, Properties, Applications*, John Wiley & Sons, ISBN 0-47149-748-6, West Sussex, England.

Neilson, S.W. (1957). Effect of strong shocks in ferroelectric materials. *Bulletin of the American Physical Society,* Vol. 2, No. 2, (March 1957) pp. 302-302, ISSN 0361-2228.

Novitskii, E.Z., Sadunov, V.D. & Karpenko, G.A. (1978). Behavior of ferroelectrics in shock waves. *Combustion, Explosion, and Shock Waves*, Vol. 14, No. 4, (July 1977), pp. 505-516, ISSN 0010-5082.

Novitskii, E.Z. & Sadunov, V.D. (1985). Behavior of ferroelectrics in shock waves. *Combustion, Explosion, and Shock Waves*, Vol. 21, No. 5, (May 1985), pp. 611-615, ISSN 0010-5082.

Online A. Available: www.teledynerisi.com

Online B. Available: www.defense.itt.com

Reynolds, C. E. & Seay, G. E. (1961). Multiple shock wave structures in polycrystalline ferroelectrics. *Journal of Applied Physics*, Vol. 32, No. 7, (July 1961) pp. 1401-1402, ISSN 0021-8979.

Reynolds, C. E. & Seay, G. E. (1962). Two-wave shock structures in the ferroelectric ceramics barium titanate and lead zirconate titanate. *Journal of Applied Physics*, Vol. 33, No. 7, (July 1962) pp. 2234-2241, ISSN 0021-8979.

Setchell, R.E. (2003). Shock wave compression of the ferroelectric ceramic $Pb_{0.99}(Zr_{0.95}Ti_{0.05})_{0.98}Nb_{0.02}O_3$: Hugoniot states and constitutive mechanical properties. *Journal of Applied Physics*, Vol. 94, No. 1, (July 2003) pp. 573-588, ISSN 0021-8979.

Setchell, R.E. (2005). Shock wave compression of the ferroelectric ceramic $Pb_{0.99}(Zr_{0.95}Ti_{0.05})_{0.98}Nb_{0.02}O_3$: Depoling currents. *Journal of Applied Physics*, Vol. 97, No. 1, (January 2005), Article number 013507, ISSN 0021-8979.

Setchell, R.E., Montgomery, S.T., Cox, D.E. & Anderson, M.U. (2006). Dielectric properties of PZT 95/5 during shock compression under high electric fields. *AIP Conference Proceedings*, Vol. 845, Part 1, (August 2006) pp. 278-281, ISBN 0-7354-0341-4.

Setchell R.E. (2007). Shock wave compression of the ferroelectric ceramic $Pb_{0.99}(Zr_{0.95}Ti_{0.05})_{0.98}Nb_{0.02}O_3$: Microstructural effect. *Journal of Applied Physics*, Vol. 101, No. 5, (March, 2007) Article number 053525, ISSN 0021-8979.

Shkuratov, S.I., Talantsev, E.F., Dickens, J.C. & Kristiansen, M. (2002a). Transverse shock wave demagnetization of $Nd_2Fe_{14}B$ high-energy hard ferromagnetics. *Journal of Applied Physics*, Vol. 92, No. 1, (July 2002) pp. 159-162, ISSN 0021-8979.

Shkuratov, S.I., Talantsev, E.F., Dickens, J.C. & Kristiansen, M. (2002b). Ultracompact explosive-driven high-current source of primary power based on shock wave demagnetization of $Nd_2Fe_{14}B$ hard ferromagnetics. *Review of Scientific Instruments*, Vol. 73, No. 7, (July 2002) pp. 2738-2741, ISSN 0034-6748.

Shkuratov, S.I., Talantsev, E.F., Dickens, J.C. & Kristiansen, M. (2002c). Compact explosive-driven generator of primary power based on a longitudinal shock wave demagnetization of hard ferri- and ferromagnets. *IEEE Transactions on Plasma Science*, Vol. 30, No. 5, (October 2002) pp. 1681-1691, ISSN 0093-3813.

Shkuratov, S.I., Talantsev, E.F., Dickens, J.C., Kristiansen, M. & Baird, J. (2003a). Longitudinal-shock-wave compression of $Nd_2Fe_{14}B$ high-energy hard ferromagnet: The pressure-induced magnetic phase transition. *Applied Physics Letters*, Vol. 82, No. 8, (February 2003) pp. 1248-1250, ISSN 0003-6951.

Shkuratov, S.I., Talantsev, E.F., Dickens, J.C. & Kristiansen, M., (2003b). Currents produced by explosive driven transverse shock wave ferromagnetic source of primary power in a coaxial single-turn seeding coil of a magnetocumulative generator. *Journal of Applied Physics*, Vol. 93, No. 8, (April 2003) pp. 4529-4535, ISSN 0021-8979.

Shkuratov, S.I., Talantsev, E.F., Menon, L., Temkin, H., Baird, J. & Altgilbers, L.L. (2004). Compact high-voltage generator of primary power based on shock wave depolarization of lead zirconate titanate piezoelectric ceramics. *Review of Scientific Instruments*, Vol. 75, No. 8, (August 2004) pp. 2766-2769, ISSN 0034-6748.

Shkuratov, S.I., Talantsev, E.F., Baird, J., Rose, M.F., Shotts, Z., Altgilbers, L.L. & Stults, A.H. (2006a). Completely explosive ultracompact high-voltage nanosecond pulse-generating system. *Review of Scientific Instruments*, Vol. 77, No. 4, (April, 2006) Article number 043904, ISSN 0034-6748.

Shkuratov, S.I., Talantsev, E.F., Baird, J., Altgilbers, L.L. & Stults, A.H. (2006b). Compact autonomous explosive-driven pulsed power system based on a capacitive energy storage charged by a high-voltage shock-wave ferromagnetic generator. *Review of Scientific Instruments*, Vol. 77, No. 6, (June, 2006) Article number 066107, ISSN 0034-6748.

Shkuratov, S.I., Talantsev, E.F., Baird, J., Temkin, H., Altgilbers, L.L. & Stults, A.H. (2006c). Longitudinal shock wave depolarization of $Pb(Zr_{0.52}Ti_{0.48})O_3$ polycrystalline ferroelectrics and their utilization in explosive pulsed power," *AIP Conference Proceedings*, Vol. 845, Part 2, (August 2006) pp. 1169-1172, ISBN 0-7354-0341-4.

Shkuratov, S.I., Baird, J., Talantsev, E.F., Rose, M.F., Shotts, Z., Altgilbers, L.L., Stults, A.H. & Kolossenok, S.V. (2007a). Completely explosive ultracompact high-voltage pulse generating system. *Digest of Technical Papers-IEEE International Pulsed Power Conference*, pp. 445-448, ISBN 978-078039190-1, Monterey, CA, June 2005, IEEE, Piscataway.

Shkuratov, S.I., Talantsev, E.F., Baird, J., Temkin, H., Tkach, Y., Altgilbers, L.L. & Stults, A.H. (2007b). The depolarization of a $Pb(Zr_{0.52}Ti_{0.48})O_3$ polycrystalline piezoelectric energy-carrying element of compact pulsed power generator by a longitudinal shock wave. *Digest of Technical Papers-IEEE International Pulsed Power Conference*, pp. 529-532, ISBN 978-078039190-1, Monterey, CA, June 2005, IEEE, Piscataway.

Shkuratov, S.I., Baird, J., Talantsev, E.F., Tkach, Y., Altgilbers, L.L., Stults, A.H. & Kolossenok, S.V. (2007c). Pulsed charging of capacitor bank by compact explosive-driven high-voltage primary power source based on longitudinal shock wave depolarization of ferroelectric ceramics. *Digest of Technical Papers-IEEE International Pulsed Power Conference*, pp. 537-540, ISBN 978-078039190-1, Monterey, CA, June 2005, IEEE, Piscataway.

Shkuratov, S.I., Talantsev, E.F., Baird, J., Ponomarev, A.V., Altgilbers, L.L. & Stults, A.H. (2007d). Operation of the longitudinal shock wave ferroelectric generator charging a capacitor bank: Experiments and digital model. *PPPS-2007 - Pulsed Power Plasma Science 2007*, pp. 1146-1150, ISBN 978-142440914-3, Albuquerque, NM, June 2007, IEEE, Piscataway.

Shkuratov, S.I., Baird, J., Talantsev, E.F., Ponomarev, A.V., Altgilbers, L.L., & Stults, A.H. (2008a). High-voltage charging of a capacitor bank. *IEEE Transactions on Plasma Science*, Vol. 36, No. 1, (February 2008) pp. 44-51, ISSN 0093-3813.

Shkuratov, S.I., Talantsev, E.F., Baird, J., Altgilbers, L.L. & Stults, A.H. (2008b). Pulse charging of capacitor bank by explosive-driven shock wave ferroelectric generator. *2006 International Conference on Megagauss Magnetic Field Generation and Related Topics, including the International Workshop on High Energy Liners and High Energy Density Applications, MEGAGAUSS*, pp. 325-330, ISBN 978-142442061-2, Santa Fe, NM, November 2006, IEEE, Piscataway.

Shkuratov, S.I., Baird, J., Antipov, V.G., Talantsev, E.F., Lynch, C.S. & Altgilbers, L.L. (2010). Depolarization of PZT 52/48: Longitudinal explosive shock versus quasi-static thermal heating. *IEEE Transactions on Plasma Science*, accepted for publication. ISSN 0093-3813.

Shur, V.Ya., Negashev, S.A., Subbotin, A.L. & Borisova, E.A. (1997). Crystallization kinetics of amorphous ferroelectric films. *Ferroelectrics*, Vol. 196, No. 1-4, (January 1997) pp. 183-186, ISSN 0015-0193.

Tkach, Y., Shkuratov, S.I., Talantsev, E.F., Dickens, J.C., Kristiansen, M., Altgilbers, L.L. & Tracy, P.T. (2002). Theoretical treatment of explosive-driven ferroelectric generators. *IEEE Transactions on Plasma Science*, Vol. 30, No. 5, (October 2002) pp. 1665-1673, ISSN 0093-3813.

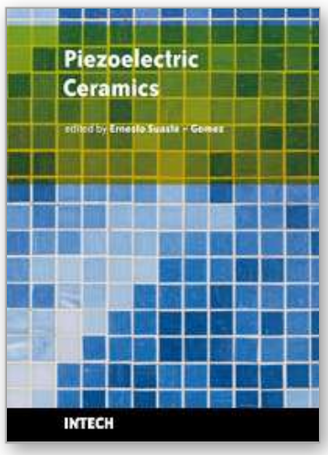

Piezoelectric Ceramics

Edited by Ernesto Suaste-Gomez

ISBN 978-953-307-122-0

Hard cover, 294 pages

Publisher Sciyo

Published online 05, October, 2010

Published in print edition October, 2010

This book reviews a big window of opportunity for piezoelectric ceramics, such as new materials, material combinations, structures, damages and porosity effects. In addition, applications of sensors, actuators, transducers for ultrasonic imaging, positioning systems, energy harvesting, biomedical and microelectronic devices are described. The book consists of fourteen chapters. The genetic algorithm is used for identification of RLC parameters in the equivalent electrical circuit of piezoelectric transducers. Concept and development perspectives for piezoelectric energy harvesting are described. The characterization of principal properties and advantages of a novel device called ceramic-controlled piezoelectric with a Pt wire implant is included. Bio-compatibility studies between piezoelectric ceramic material and biological cell suspension are exposed. Thus, piezoelectric ceramics have been a very favorable solution as a consequence of its high energy density and the variety of fabrication techniques to obtain bulk or thin films devices. Finally, the readers will perceive a trend analysis and examine recent developments in different fields of applications of piezoelectric ceramics.

InTech Europe
University Campus STeP Ri
Slavka Krautzeka 83/A
51000 Rijeka, Croatia
Phone: +385 (51) 770 447
Fax: +385 (51) 686 166
www.intechopen.com

InTech China
Unit 405, Office Block, Hotel Equatorial Shanghai
No.65, Yan An Road (West), Shanghai, 200040, China
中国上海市延安西路65号上海国际贵都大饭店办公楼405单元
Phone: +86-21-62489820
Fax: +86-21-62489821

IntechOpen